

Algorithms For Shaping a Particle Swarm With a Shared Control Input Using Boundary Interaction*

Shiva Shahrokhi, Arun Mahadev, and Aaron T. Becker

Abstract—There are driving applications for large populations of tiny robots in robotics, biology, and chemistry. These robots often lack onboard computation, actuation, and communication. Instead, these “robots” are particles carrying some payload and the particle swarm is controlled by a shared, global control input such as a uniform magnetic gradient or electric field. In previous work, we showed that the 2D position of each particle in such a swarm is controllable if the workspace contains a single obstacle the size of one particle.

Requiring a small, rigid obstacle suspended in the middle of the workspace is a strong constraint, especially in 3D. This paper relaxes that constraint, and provides position control algorithms that only require interactions with the boundaries. Both *in vivo* and artificial environments often have boundaries. We assume that particles in contact with the boundaries have zero velocity if the global control input pushes the particle into the wall. This paper provides an optimal shortest-path algorithm for positioning a two-particle swarm, and a generalization to positioning an n -particle swarm. Results are validated with simulations and a hardware demonstration.

I. INTRODUCTION

Particle swarms propelled by a global field, where each particle receives the same control input, are common in applied mathematics, biology, and computer graphics. As a current example, micro- and nano-robots can be manufactured in large numbers, see [3]–[9]. Someday large swarms of robots will be remotely guided to assemble structures in parallel and through the human body to cure disease, heal tissue, and prevent infection. For each task, large numbers of micro robots are required to deliver sufficient payloads, but the small size of these robots makes it difficult to perform onboard computation. Instead, these robots are often controlled by a global, broadcast signal. The tiny robots themselves are often just rigid bodies, and it may be more accurate to define the *system*, consisting of particles, a global control field, and sensing, as the robot. Such systems are severely underactuated, having 2 degrees of freedom in the shared control input, but $2n$ degrees of freedom for the particle swarm. Techniques are needed that can handle this underactuation. In previous work, we showed that the 2D position of each particle in such a swarm is controllable if the workspace contains a single obstacle the size of one particle.

Positioning is a foundational capability for a robotic system, but requiring a single, small, rigid obstacle suspended in the middle of the workspace is often an unreasonable constraint, especially in 3D. This paper relaxes that constraint,

*This work was supported by the National Science Foundation under Grant No. [IIS-1553063] and [IIS-1619278].

Authors are with the Department of Electrical and Computer Engineering, University of Houston, Houston, TX 77204 USA {sshahrokhi2, aviswanathanmahadev, atbecker}@uh.edu

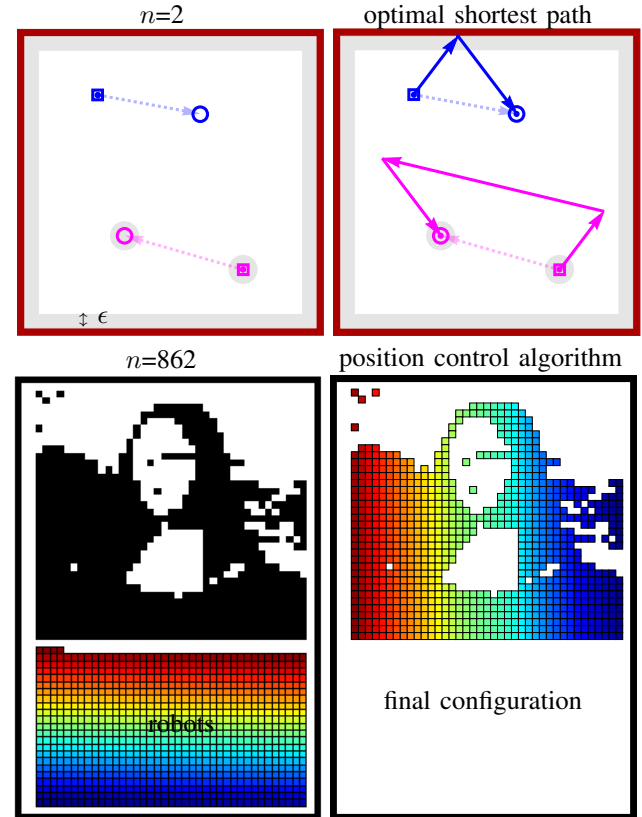


Fig. 1. Positioning particles that receive the same control inputs, but cannot move while a control input pushes them into a boundary. Top row shows the output of a dynamic algorithm that finds the shortest path for two particles. Top left shows the initial position and goal position of the particles. The shortest path consists of moving at angle 50° until the blue robot contacts the top wall, then moving the magenta robot at angle 165° until the particles reach the desired relative spacing, then moving -60° to the goal positions. The two bottom pictures shows n -particle positioning using shared control inputs and boundary interaction.

and provides position control algorithms that only require interactions with the boundaries. We assume that particles in contact with the boundaries have zero velocity if the global control input pushes the particle into the wall.

The paper is arranged as follows. After a review of recent related work in Sec. II, Sec. III introduces a model for boundary interaction. We provide an optimal shortest-path algorithm for arbitrarily position two robots in Sec. IV, and Sec. V extends this to prove a rectangular workspace with high-friction boundaries can position a swarm of n robots arbitrarily within a subset of the workspace. Sec. VI describes implementations of the algorithms in simulation and Sec. VII describes hardware experiments, as shown in

Fig. 1. We end with directions for future research in Sec. VIII.

II. RELATED WORK

Controlling the *shape*, or relative positions, of a swarm of robots is a key ability for a range of applications. Correspondingly, it has been studied from a control-theoretic perspective in both centralized and decentralized approaches. For examples of each, see the centralized virtual leaders in [11], and the gradient-based decentralized controllers using control-Lyapunov functions in [12]. However, these approaches assume a level of intelligence and autonomy in individual robots that exceeds the capabilities of many systems, including current micro- and nano-robots. Current micro- and nano-robots, such as those in [3], [13], [14] lack onboard computation.

Instead, this paper focuses on centralized techniques that apply the same control input to each member of the swarm. Precision control requires breaking the symmetry caused by the global input. Symmetry can be broken using agents that respond differently to the global control, either through agent-agent reactions, see work modeling biological swarms [15], or engineered inhomogeneity [6], [16], [17]. This work assumes a uniform control with homogenous agents, as in [18]. The techniques in this paper are inspired by artificial force-fields.

Artificial Force-fields: Much research has focused on generating non-uniform artificial force-fields that can be used to rearrange passive components. Applications have included techniques to design shear forces for sensorless manipulation of a single object by [21]. [22], [23] demonstrated a collection of 2D force fields generated by six degree-of-freedom vibration inputs to a rigid plate. These force fields, including shear forces, could be used as a set of primitives for motion control to steer the formation of multiple objects. However unlike the uniform control model in this paper, theirs was multi-modal and position-dependent.

III. THEORY

Using Boundaries: Friction and Boundary Layers

Global inputs in the absence of obstacles move a swarm uniformly. Shape control requires breaking this uniform symmetry. The following sections examine using boundaries that stop the particles if they are pushed into the wall. These forces are sufficient to break the symmetry caused by uniform inputs.

If the i^{th} particle has position $\mathbf{x}_i(t)$ and velocity $\dot{\mathbf{x}}_i(t)$, we assume the following system model:

$$\dot{\mathbf{x}}_i(t) = \mathbf{u}(t) + F(\mathbf{x}_i(t), \mathbf{u}(t)), \quad i \in [1, n].$$

$$F(\mathbf{x}_i(t), \mathbf{u}(t)) = \begin{cases} -\mathbf{u}(t) & \mathbf{x}_i(t) \in \text{boundary and} \\ & \mathbf{N}(\text{boundary}(\mathbf{x}_i(t))) \cdot \mathbf{u}(t) \leq 0 \\ 0 & \text{else} \end{cases}$$

Here $\mathbf{N}(\text{boundary}(\mathbf{x}_i(t)))$ is the normal to the boundary at position $\mathbf{x}_i(t)$, and $F(\mathbf{x}_i(t), \mathbf{u}(t))$ is the frictional force provided by the boundary.

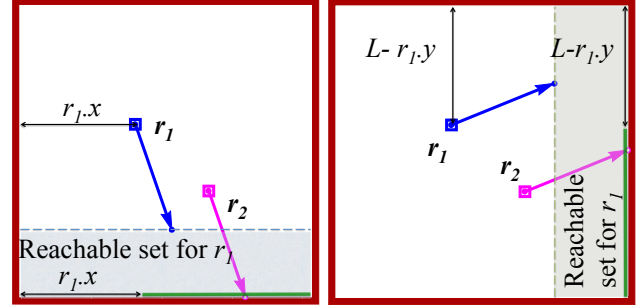


Fig. 2. Boundary interaction is used to change relative position. Each robot gets the same control input. (left) If robot 2 hits the bottom wall before robot 1 reaches a wall, robot 2 can reach anywhere along the green line, and robot 1 can move to anywhere in the shaded area. (right) Similarly, if robot 2 hits the right wall before robot 1 reaches a wall, robot 2 can reach anywhere along the green line, and robot 1 can move to anywhere in the shaded area.

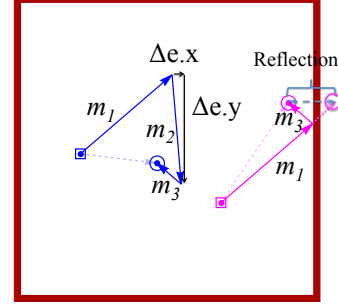


Fig. 5. If the goal configuration can be reached in three moves, the first move makes one particle hit a wall, the second move adjusts the relative spacing error Δe to zero, and the third move takes the particles to their final positions. The second move cannot be shortened, so optimization depends on choosing the location where the robot hits the wall. Since the shortest distance between two points is a straight line, reflecting the goal position across the boundary wall and plotting a straight line gives the optimal hit location.

These system dynamics represent particle swarms in low-Reynolds number environments, where viscosity dominates inertial forces and so velocity is proportional to input force [1]. In this regime, the input force command $\mathbf{u}(t)$ controls the velocity of the robots. The same model can be generalized to particles moved by fluid flow where the vector direction of fluid flow $\mathbf{u}(t)$ controls the velocity of particles, or for a swarm of robots that move at a constant speed in a direction specified by a global input $\mathbf{u}(t)$ [2]. Our control problem is to design the control inputs $\mathbf{u}(t)$ to make all n particles achieve a task.

IV. POSITION CONTROL OF TWO ROBOTS USING WALL FRICTION

Alg. 1 uses wall-friction to arbitrarily position two robots in a rectangular workspace. This algorithm introduces concepts that will be used for multi-robot positioning. Fig. 6 shows a Mathematica implementation of the algorithm, and is useful as a visual reference for the following description.

Assume two robots are initialized at r_1 and r_2 with corresponding goal destinations g_1 and g_2 . We can exploit symmetry in the solution by labeling the leftmost (or, if they have the same x coordinate, the topmost) robot r_1 . If r_1 is not also the topmost robot, we mirror the coordinate frame across

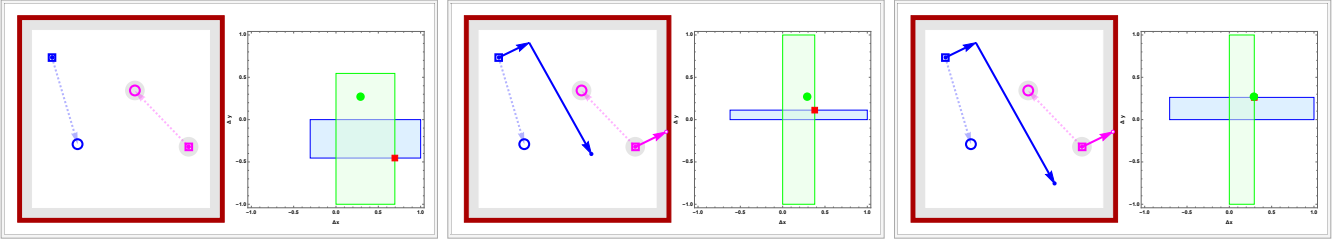


Fig. 3. Workspace and Δ configuration space for three sets of robot configurations with the same final goal. The red square represents the starting Δx and Δy and the green circle represents the goal Δx and Δy . The green rectangle illustrates one move reachable Δx and Δy by horizontal walls and the blue rectangle illustrates the vertical walls reachable region.

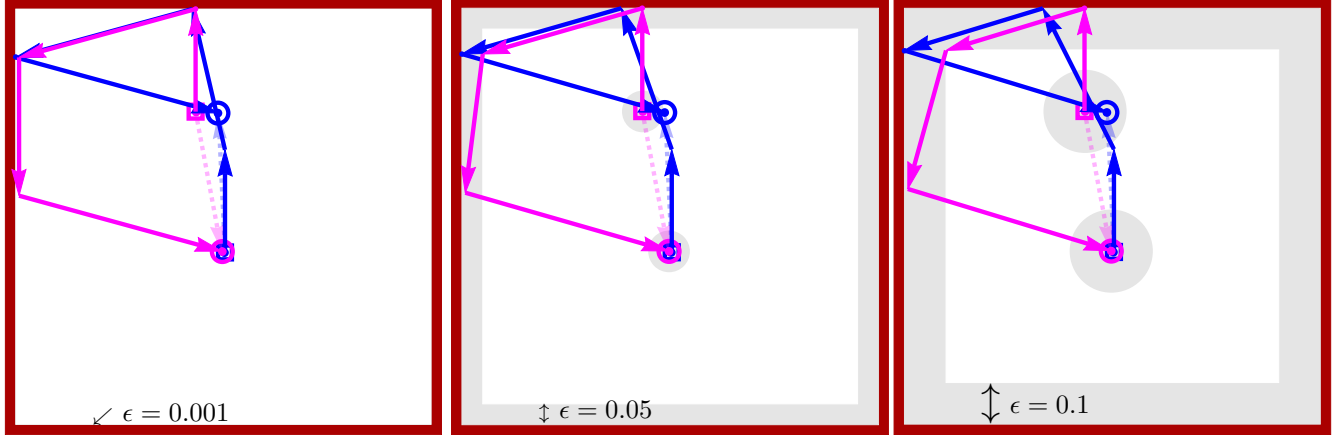


Fig. 4. Changing the minimum spacing ϵ changes the path. ϵ is the minimum spacing between two robots and the minimum separation from the boundaries.

the right wall. To give an example to understand mirroring, consider the two starting positions, $r_1 = (0.2, 0.2)$ and $r_2 = (0.8, 0.8)$. Because the leftmost robot is not the topmost robot, we mirror the coordinate frame giving $r_1 = (0.2, 0.8)$ and $r_2 = (0.8, 0.2)$. We do this to reuse the main algorithm's logic and after the path is found, we undo the mirroring to the output path. Similarly, we exploit rotational symmetry and assume the command pushes a robot to hit the top wall. If a different wall is selected, we rotate the coordinate frame by 90° , 180° or 270° counterclockwise to get other walls paths and translate the path after the algorithm returns the path for the rotated coordinate frame.

Denote the current positions of the robots r_1 and r_2 . Values $.x$ and $.y$ denote the x and y coordinates, i.e., $r_1.x$ and $r_1.y$ denote the x and y locations of r_1 . The algorithm assigns a global control input at every instance. The goal is to adjust the error in both coordinates, $\Delta e = (\Delta e.x, \Delta e.y) = \Delta g - \Delta r = (g_2 - g_1) - (s_2 - s_1)$ to $(0, 0)$ using a shared global control input. Our algorithm uses a A* like method of dynamic search to find the shortest path in each move. The base case occurs when $\Delta e = (0, 0)$. In this base case, the shortest path is a straight line between current position of each robot to its goal position, see Fig. 6 a. If $\Delta e \neq (0, 0)$, we consult the two-move reachable sets shown in Fig. 3. If a robot is touching a wall, the other robot can move to any position in the reachable set while the first robot is immobile. Two reachable sets are possible, horizontal and vertical. If $(\Delta g.x, \Delta g.y)$ is in the reachable set, one robot touches a wall and the other robot zeros the error in one move. This is

shown as m_2 in Fig. 5. To find the best place to minimize m_1 and m_3 , the touching robot's goal is reflected on that wall. The minimum distance to get to the goal in two move when the robot should touch the wall, is the straight line between the robot and the reflection of the goal position on that wall. That point is selected when possible, but if it makes m_2 reach out of the workspace, the closest point to this point where the moving robot would not get out of the workspace is selected.

If $(\Delta g_x, \Delta g_y)$ is not in the reachable set, we choose the nearest Δx and Δy to Δg_x and Δg_y and reach there. In this step for simplicity we choose the straight line from the touching robot to the wall for the first move. This may cause the algorithm not to return the shortest path, but the difference is not significant. Alg. 1 returns the total distance of the path added to the euclidian distance of the final position of the robots to their goal. We use euclidian distance as a heuristic to find the path faster.

Alg. 2 is a dynamic search to find the shortest path by all the walls. It keeps a list containing all the possible paths with their current and final position of the robots. At each iteration, the algorithm sorts all the paths in the list by their total distance plus heuristic. It picks the shortest path, and calls Alg. 1 for all the four walls. It keeps calling and sorting until the goal has reached. When the goal is reached, the algorithm returns the shortest path and the final solution.

In the worse case, adjusting both Δr_x and Δr_y needs all four steps. If we consider the length of each side of the square workspace as L , the worst case path length is $(\sqrt{2} + 2)L$.

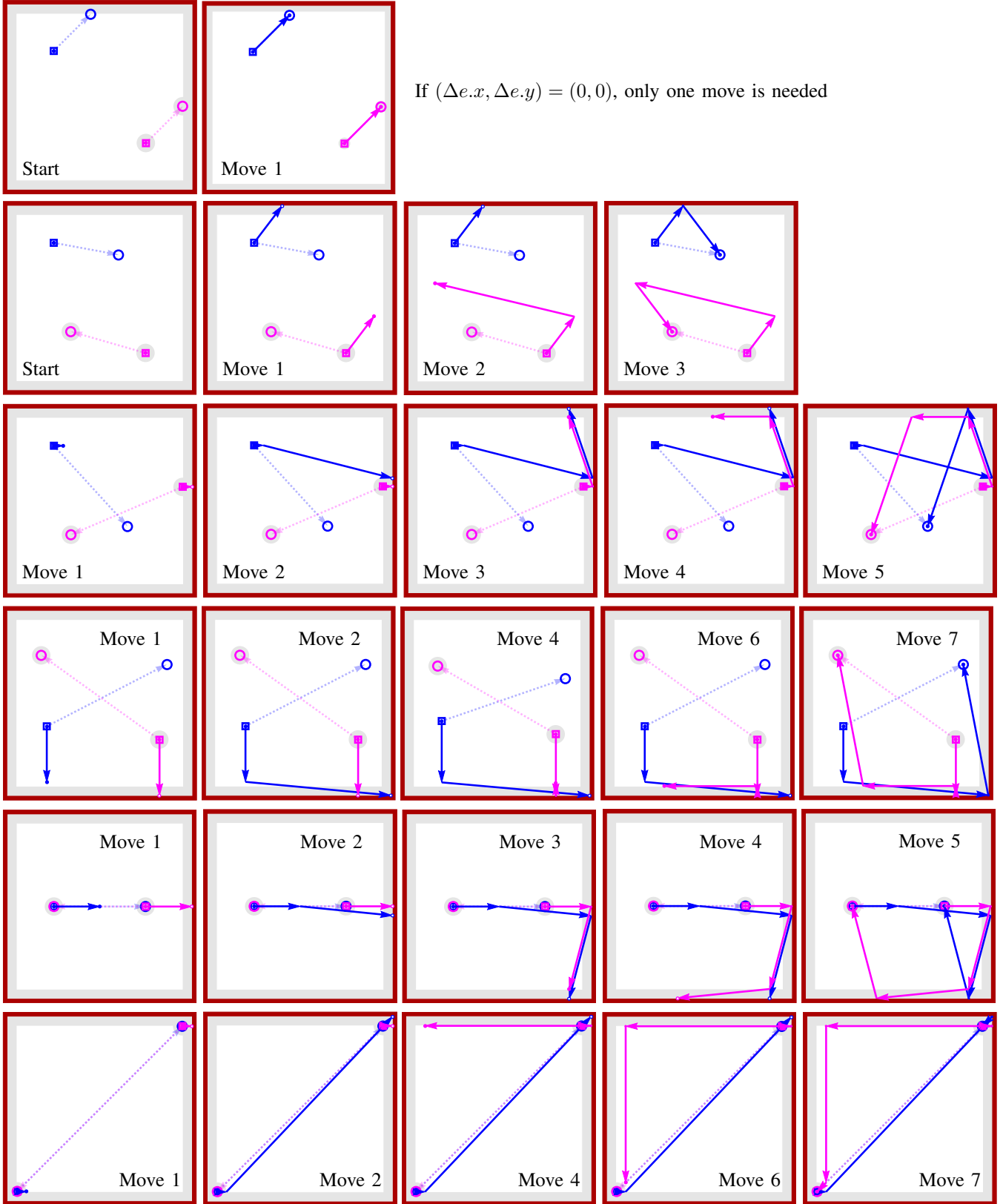


Fig. 6. Frames from an implementation of Alg. 2: two robot positioning using walls with infinite friction. Robot start positions are shown by a square, and goal positions by a circle. Dashed lines show the shortest route if robots could be controlled independently. Solid arrows show path given by Alg. 2. Online demonstration and source code at [25].

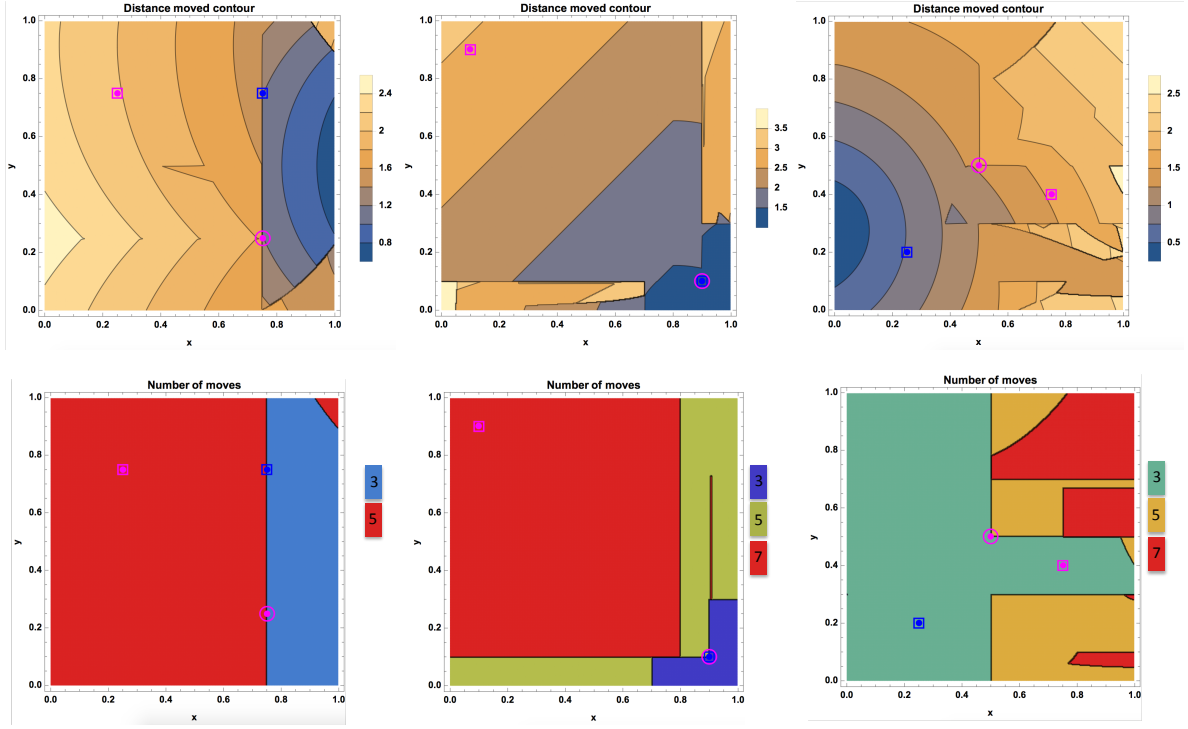


Fig. 7. Starting positions of robots 1 and 2 and goal position of robot 2 are fixed, and the contour plots calculate the distance if robot 1's goal position is varied in x and y . The second row shows the number of moves required for the same configurations.

V. POSITION CONTROL OF n ROBOTS USING WALL FRICTION

The ideas from Alg. 2 can be extended to control the position of n particles using wall friction. The solution is complete, but not optimal, and requires the starting and final configurations of particles to be disjoint. The solution described here is an iterative procedure with n loops. The k th loop moves the k th robot from a *staging zone* to the desired position in a *build zone*. All robots move according to the global input, but due to wall friction, at the end of the k th loop, robots 1 through k are in their desired final configuration in the build zone, and robots $k + 1$ to n are in the staging zone. See Fig. 8 for a schematic of the build and staging zones.

Assume an open workspace with four axis-aligned walls with infinite friction. The axis-aligned build zone of dimension (w_b, h_b) containing the final configuration of n robots must be disjoint from the axis-aligned staging zone of dimension (w_s, h_s) containing the starting configuration of n robots. Without loss of generality, assume the build zone is above the staging zone. Let d be the diameter the particles. Furthermore, there must be at least ϵ space above the build zone, ϵ below the staging zone, and $\epsilon + d$ to the left of the build and staging zone. The minimum workspace is then $(\epsilon + d + \max(w_b, w_s), 2\epsilon + h_s, h_b)$.

The n robot position control algorithm relies on a DRIFTMOVE($\alpha, \beta, \epsilon, \theta$) control input, described in Alg. 4 and shown in Fig. 9. For $\theta = 0^\circ$, a drift move consists of repeating a triangular movement sequence $\{(\beta/2, -\epsilon), (\beta/2, \epsilon), (-\alpha, 0)\}$. Any particle touching a top

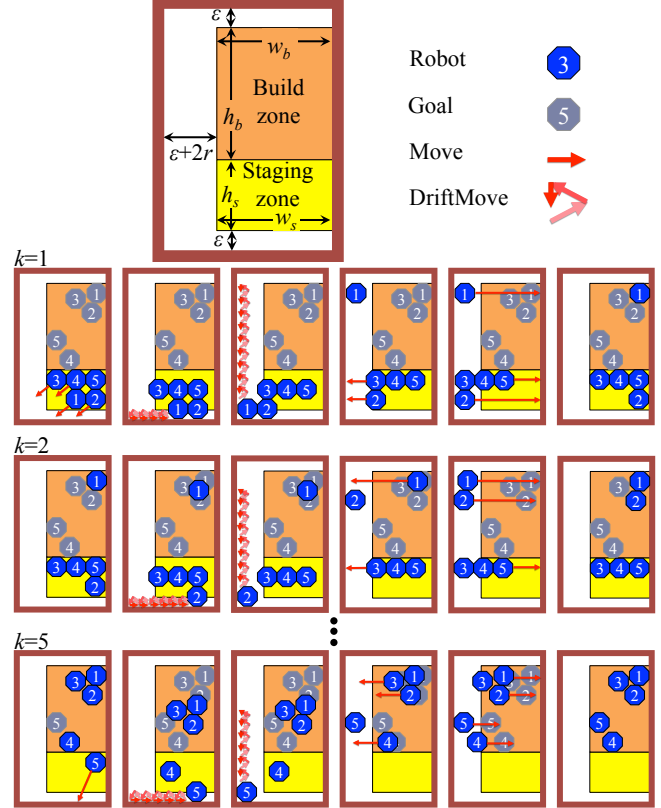


Fig. 8. Illustration of Alg. 3, n robot position control using wall friction.

Algorithm 1 WallFrictionMoveUp($r_1, r_2, g_1, g_2, L, moves$)

Require: knowledge of current (r_1, r_2) and goal (g_1, g_2) positions of two robots. (0, 0) is bottom corner, L is length of the walls. The array $moves$ is the current moves up to the current position. m_1 is the first move toward the wall or goal. m_2 is the second move adjusting Δe . Assume $r_1.x < r_2.x$ and $r_1.y \geq r_2.y$. If not, mirror the coordinate frame and swap the robots. ϵ is a small, nonzero, user-specified value.

Ensure: $(g_1, g_2), (r_1, r_2)$ all at least ϵ distance from walls the goals and starting points have at least epsilon distance from each other.

- 1: $\Delta e = (g_2 - g_1) - (r_2 - r_1)$
- 2: Admissible heuristic = max(euclidian distance from goal)
- 3: **if** $\Delta e = (0, 0)$ **then**
- 4: $m_1 = (g_2.x - r_2.x, g_2.y - r_2.y)$
- 5: path \leftarrow path + m_1
- 6: Return (total distance of path, path)
- 7: **end if**
- 8: **if** $r_2.x - r_1.x - 1 + 2\epsilon \leq \Delta g_x \leq 1 \ \&\& \ r_2.y - r_1.y \leq \Delta g_y \leq 0$ **then**
- 9: $m_1 = (\frac{1-r_1.y}{2-g_1.y-r_1.y}g_1.x - r_1.x, 1 - r_1.y)$
- 10: **if** $r_2.x + m_1.x > L$ **then**
- 11: $m_1.x = 1 - r_2.x$
- 12: **end if**
- 13: **if** $r_2.x + m_1.x < 0$ **then**
- 14: $m_1.x = -r_2.x$
- 15: **end if**
- 16: **else**
- 17: $m_1 = (0, 1 - r_1.y)$
- 18: Adjust Δg_x and Δg_y
- 19: **end if**
- 20: path \leftarrow path + m_1
- 21: $r_1 = r_1 + m_1$ and $r_2 = r_2 + m_1$
- 22: $m_2 = (\Delta g_x - (r_2.x - r_1.x), \Delta g_y - (r_2.y - r_1.y))$
- 23: **if** Robots on each other or on the wall **then**
- 24: Add $\pm\epsilon$ to $m_2.x$
- 25: **end if**
- 26: path \leftarrow path + m_2
- 27: Unmirror if necessary
- 28: Return(total distance of path + Admissible heuristic, path)

wall moves right β units, while every particle not touching the top moves right $\beta - \alpha$.

Let $(0, 0)$ be the lower left corner of the workspace, p_k the x, y position of the k th robot, and f_k the final x, y position of the k th robot. Label the robots in the staging zone from left-to-right and bottom-to-top, and the f_k configurations top-to-bottom and right-to-left as shown in Fig. 10.

Alg. 3 proceeds as follows: First, the robots are moved left away from the right wall, and down so all robots in k 's row touch the bottom wall. Second, a set of DriftMoves are executed that move all robots in k 's row left until k

Algorithm 2 DynamicOptimalSolutionFinder(r_1, r_2, g_1, g_2, L)

Require: knowledge of current (r_1, r_2) and goal (g_1, g_2) positions of two robots. (0, 0) is bottom corner, L is length of the walls. $OptimalPathList$ is a List containing all the paths sorted by their total distance.

- 1: Pop the first element in $OptimalPathList$
- 2: **while** We have not reached the goal in the first element **do**
- 3: Call Alg. 1 for all the four walls.
- 4: Add the results to $OptimalPathList$
- 5: Sort $OptimalPathList$
- 6: **end while**
- 7: Return(path)

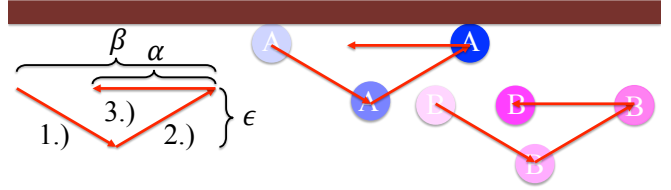


Fig. 9. A DRIFTMOVE($\alpha, \beta, \epsilon, 0^\circ$) repeats a triangular movement sequence $\{(\beta/2, -\epsilon), (\beta/2, \epsilon), (-\alpha, 0)\}$. Robot A touching a top wall moves right β units, while robots not touching the top move right $\beta - \alpha$.

Algorithm 3 PositionControlInRobotsUsingWallFriction(k)

- 1: Move($-\epsilon, d/2 - p_{ky}$)
- 2: **while** $p_{kx} > d/2$ **do**
- 3: DRIFTMOVE($\epsilon, \min(p_{kx} - d/2, \epsilon), \epsilon, 180^\circ$)
- 4: **end while**
- 5: $m \leftarrow \text{ceil}(\frac{f_{ky}-d/2}{\epsilon})$
- 6: $\beta \leftarrow \frac{f_{ky}-d/2}{m}$
- 7: $\alpha \leftarrow \beta - \frac{d/2-p_{ky}-\epsilon}{m}$
- 8: **for** m iterations **do**
- 9: DRIFTMOVE($\alpha, \beta, \epsilon, 90^\circ$)
- 10: **end for**
- 11: Move($d/2 + \epsilon - f_{kx}, 0$)
- 12: Move($f_{kx} - d/2, 0$)

Algorithm 4 DRIFTMOVE($\alpha, \beta, \epsilon, \theta$)

particles touching the wall move β units, while particles not touching the wall move $\beta - \alpha$ units.

- 1: $R = \begin{bmatrix} \cos(\theta) & -\sin(\theta) \\ \sin(\theta) & \cos(\theta) \end{bmatrix}$
- 2: MOVE($R \cdot [\beta/2, -\epsilon]^\top$)
- 3: MOVE($R \cdot [\beta/2, \epsilon]^\top$)
- 4: MOVE($R \cdot [-\alpha, 0]^\top$)

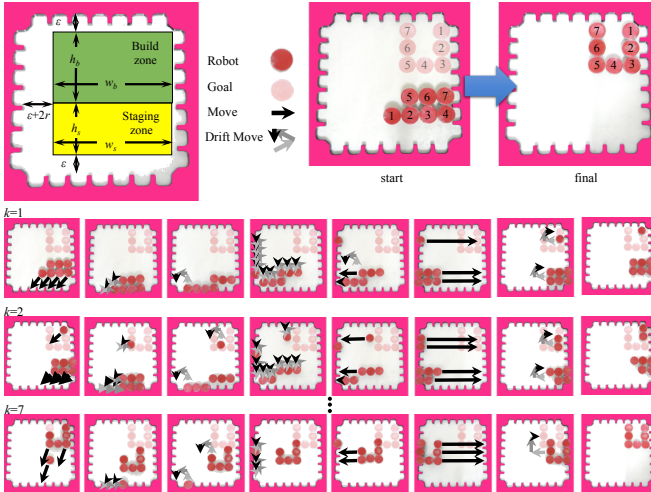


Fig. 10. Illustration of Alg. 3, discretized n robot position control using wall friction.

touches the left wall, with no net movement of the other robots. Third, a set of DriftMoves are executed that move only robot k to its target height and return the other robots to their initial heights. Fourth, all robots except robot k are pushed left until robot k is in the correct relative x position compared to robots 1 to $k - 1$. Finally, all robots are moved right until robot k is in the desired target position. Running time is $O(n(w + h))$.

The hardware platform depicted in 10 is an assembled practical setup that assumes that $\epsilon = 1$ cm. The workspace is a 7×7 cm grid space. All particles are 3D-printed plastic whose top is a 1cm diameter cylinder with a narrower base that encapsulates a steel bearing ball. Wall friction is emulated by a toothed wall design to keep particles from moving out of place while implementing the drift move. The workspace boundary is mounted on top of a white sheet of cardboard. Underneath the cardboard, a grid of 3mm diameter magnets glued with 1 cm spacing to a thin board generates the global control input. A video attachment shows the algorithm at work. This discretized setup requires several modifications to Alg. 3. In this demonstration, all moves are 1 cm in length. All drift moves are an counterclockwise *square* move of size 1 cm \times 1 cm. Once the k th roller gets to its designated location in each loop, a correction step is implemented. This correction step increases by two the total number of moves required per particle. Fig. 8 shows there are only 6 stages per particle involved in Alg. 3. The fixed step algorithm requires 8 stages per particle as shown in Fig. 10.

A significant difference between Alg. 3 and the fixed move implementation of it is that Alg. 3 enables placing particles at arbitrary, non-overlapping locations, while the fixed move implementation requires goal locations at the center of grid cells.

VI. SIMULATION

Two simulations were implemented using wall-friction for position control. The first controls the position of two robots, the second controls the position of n robots.

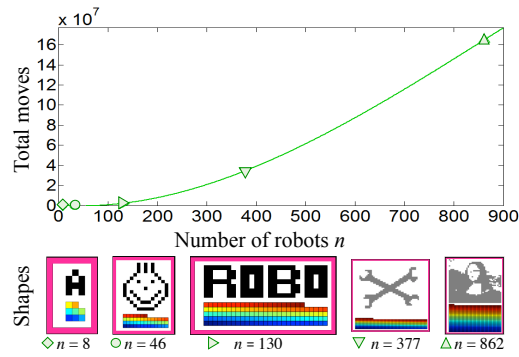


Fig. 11. The required number of moves under Alg. 3 using wall-friction to rearrange n square-shaped robots grows quadratically with n . See hardware implementation and simulation at [26].

A. Position Control of Two Robots

Algorithm ?? was implemented in Mathematica using point robots (radius = 0). Fig. 6 shows an implementation of this algorithm with robot initial positions represented by hollow squares and final positions by circles. Dashed lines show the shortest route if robots could be controlled independently, while solid lines show the optimal shortest path using uniform inputs.

The contour plots in Fig. ?? show the length of the shortest path for given s_1, s_2, g_1 with g_2 ranging over all the workspace. This plot clearly shows the nonlinear nature of the path planning, with multiple isolate islands showing regions that are difficult to reach. The contour plots in Fig. ?? show the same configurations, but plot the required number of moves. There is never more than one g_2 position reachable in one move. If two-move solutions exist, they only appear along the boundary. If g_2 results in a contraction of $(\delta x, \delta y)$, there are many three move sequences. Four-move and six-move sequences are absent, but five and seven moves are sometimes required.

B. Position Control of n Robots

Alg. 3 was simulated in MATLAB using square block robots with unity width. Code is available at [26]. Simulation results are shown in Fig. 11 for arrangements with an increasing number of robots, $n = [8, 46, 130, 390, 862]$. The distance moved grows quadratically with the number of robots n . A best-fit line $210n^2 + 1200n - 10,000$ is overlaid by the data.

In Fig. 11, the amount of clearance is $\epsilon = 1$. Control performance is sensitive to the desired clearance. As ϵ increases, the total distance decreases asymptotically, as shown in Fig. 12, because the robots have more room to maneuver and fewer DriftMoves are required.

VII. EXPERIMENT

A. Hardware Experiment: Position Control of n Robots

A hardware setup with a bounded platform, magnetic sliders, and a magnetic guide board was used to implement Alg. 3. Designs for each are available at [27]. The pink boundary is toothed with a white free space, as shown in

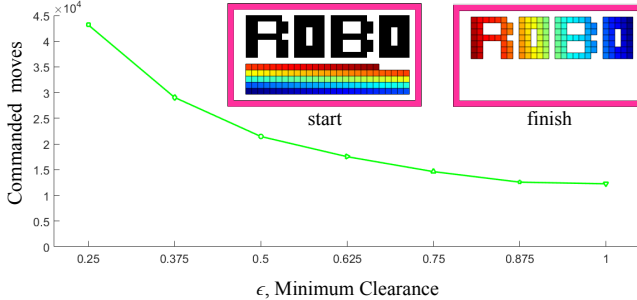


Fig. 12. Control performance is sensitive to the desired clearance ϵ . As ϵ increases, the total distance decreases asymptotically.

Fig 10. Only discrete, 1 cm moves in the x and y directions are used. The goal configuration highlighted in the top right corner represents a ‘U’ made of seven sliders. The dark red configuration is the current position of the sliders. Due to the discretized movements allowed by the boundary, drift moves follow a 1 cm square. Free robots return to their start positions but robots on the boundary to move laterally, generating a net sliding motion.

Fig. 10 follows the motion of the sliders through iterations $k=1, 2$, and 7 . All robots receive the same control inputs, but boundary interactions break the control symmetry. Robots reach their goal positions in a first-in, first-out arrangement beginning with the bottom-left robot from the staging zone occupying the top-right position of the build zone.

VIII. CONCLUSION AND FUTURE WORK

This paper presented techniques for controlling the position of a swarm of robots using uniform global inputs and interaction with boundary friction forces. The paper provided algorithms for precise position control, as well as robust and efficient covariance control. Extending algorithms ?? and 3 to 3D is straightforward but increases the complexity. Additionally, this paper assumed friction was sufficient to completely stop particles in contact with the boundary. The algorithms require retooling to handle small friction coefficients. The algorithms assumed a rectangular workspace. This is a reasonable assumption for artificial environments, but *in vivo* environments are curved. A dynamic program could still work, but it cannot take advantage of the 4-fold rotational symmetry as in a rectangular environment. Future efforts should be directed toward improving the technology and tailoring it to specific robot applications.

REFERENCES

- [1] E. M. Purcell, “Life at low reynolds number,” *American Journal of Physics*, vol. 45, no. 1, pp. 3–11, 1977. [Online]. Available: <http://dx.doi.org/10.1119/1.10903>
- [2] M. Rubenstein, C. Ahler, and R. Nagpal, “Kilobot: A low cost scalable robot system for collective behaviors,” in *IEEE Int. Conf. Rob. Aut.*, May 2012, pp. 3293–3298.
- [3] S. Chowdhury, W. Jing, and D. J. Cappelleri, “Controlling multiple microrobots: recent progress and future challenges,” *Journal of Micro-Bio Robotics*, vol. 10, no. 1-4, pp. 1–11, 2015.
- [4] S. Martel, S. Taherkhani, M. Tabrizian, M. Mohammadi, D. de Lanauze, and O. Felfoul, “Computer 3d controlled bacterial transports and aggregations of microbial adhered nano-components,” *Journal of Micro-Bio Robotics*, vol. 9, no. 1-2, pp. 23–28, 2014.
- [5] P. S. S. Kim, A. Becker, Y. Ou, A. A. Julius, and M. J. Kim, “Imparting magnetic dipole heterogeneity to internalized iron oxide nanoparticles for microorganism swarm control,” *Journal of Nanoparticle Research*, vol. 17, no. 3, pp. 1–15, 2015.
- [6] B. R. Donald, C. G. Levey, I. Paprotny, and D. Rus, “Planning and control for microassembly of structures composed of stress-engineered mems microrobots,” *The International Journal of Robotics Research*, vol. 32, no. 2, pp. 218–246, 2013.
- [7] A. Ghosh and P. Fischer, “Controlled propulsion of artificial magnetic nanostructured propellers,” *Nano Letters*, vol. 9, no. 6, pp. 2243–2245, 2009.
- [8] Y. Ou, D. H. Kim, P. Kim, M. J. Kim, and A. A. Julius, “Motion control of magnetized tetrahymena pyriformis cells by magnetic field with model predictive control,” *Int. J. Rob. Res.*, vol. 32, no. 1, pp. 129–139, Jan. 2013.
- [9] F. Qiu and B. J. Nelson, “Magnetic helical micro-and nanorobots: Toward their biomedical applications,” *Engineering*, vol. 1, no. 1, pp. 21–26, 2015.
- [10] S. Shahrokh and A. T. Becker, “Stochastic swarm control with global inputs,” in *Intelligent Robots and Systems (IROS), 2015 IEEE/RSJ International Conference on*, Sep. 2015, pp. 421–427.
- [11] M. Egerstedt and X. Hu, “Formation constrained multi-agent control,” *IEEE Trans. Robotics Automat.*, vol. 17, pp. 947–951, 2001.
- [12] M. A. Hsieh, V. Kumar, and L. Chaimowicz, “Decentralized controllers for shape generation with robotic swarms,” *Robotica*, vol. 26, no. 05, pp. 691–701, 2008.
- [13] S. Martel, “Magnetotactic bacteria for the manipulation and transport of micro-and nanometer-sized objects,” *Micro-and Nanomanipulation Tools*, pp. 308–317, 2015.
- [14] X. Yan, Q. Zhou, J. Yu, T. Xu, Y. Deng, T. Tang, Q. Feng, L. Bian, Y. Zhang, A. Ferreira, and L. Zhang, “Magnetite nanostructured porous hollow helical microswimmers for targeted delivery,” *Advanced Functional Materials*, vol. 25, no. 33, pp. 5333–5342, 2015.
- [15] A. L. Bertozzi, T. Kolokolnikov, H. Sun, D. Uminsky, and J. Von Brecht, “Ring patterns and their bifurcations in a nonlocal model of biological swarms,” *Communications in Mathematical Sciences*, vol. 13, no. 4, pp. 955–985, 2015.
- [16] T. Bretl, “Control of many agents using few instructions,” in *Proceedings of Robotics: Science and Systems*, Atlanta, GA, USA, June 2007, pp. 1–8.
- [17] A. Becker, C. Onyuksel, T. Bretl, and J. McLurkin, “Controlling many differential-drive robots with uniform control inputs,” *Int. J. Robot. Res.*, vol. 33, no. 13, pp. 1626–1644, 2014.
- [18] A. Becker, G. Habibi, J. Werfel, M. Rubenstein, and J. McLurkin, “Massive uniform manipulation: Controlling large populations of simple robots with a common input signal,” in *IEEE/RSJ International Conference on Intelligent Robots and Systems (IROS)*, Nov. 2013, pp. 520–527.
- [19] B. R. Munson, A. P. Rothmayer, T. H. Okiishi, and W. W. Huebsch, *Fundamentals of Fluid Mechanics*, 7th ed. Wiley, 2012.
- [20] D. Spears, W. Kerr, and W. Spears, “Physics-based robot swarms for coverage problems,” *The international journal of intelligent control and systems*, vol. 11, no. 3, 2006.
- [21] F. Lamiriaux and L. E. Kavraki, “Positioning of symmetric and non-symmetric parts using radial and constant fields: Computation of all equilibrium configurations,” *International Journal of Robotics Research*, vol. 20, no. 8, pp. 635–659, 2001.
- [22] T. Vose, P. Umbohanowar, and K. Lynch, “Friction-induced velocity fields for point parts sliding on a rigid oscillated plate,” *The International Journal of Robotics Research*, vol. 28, no. 8, pp. 1020–1039, 2009.
- [23] T. H. Vose, P. Umbohanowar, and K. M. Lynch, “Sliding manipulation of rigid bodies on a controlled 6-dof plate,” *The International Journal of Robotics Research*, vol. 31, no. 7, pp. 819–838, 2012.
- [24] P. J. Pritchard, *Fox and McDonald's Introduction to Fluid Mechanics*, 8th Edition. John Wiley and sons inc., 2011.
- [25] S. Shahrokh and A. T. Becker, “Moving Two Particles with Shared Control Inputs Using Wall Friction, Wolfram Demonstrations Project,” Nov. 2015. [Online]. Available: <http://demonstrations.wolfram.com/MovingTwoParticlesWithSharedControlInputsUsingWallFriction/>
- [26] A. V. Mahadev and A. T. Becker, “Arranging a robot swarm with global inputs and wall friction [discrete]. matlab central file exchange,” Dec. 2015. [Online]. Available: <https://www.mathworks.com/matlabcentral/fileexchange/54526>

- [27] A. Mahadev, A. Nguyen, and A. T. Becker, “Position control using boundary interaction,” Sep. 2016. [Online]. Available: <http://www.thingiverse.com/thing:1761909>